Research Square

Preprints are preliminary reports that have not undergone peer review.
They should not be considered conclusive, used to inform clinical practice,
or referenced by the media as validated information.

Electroacupuncture Alleviates Cerebral Ischemia-Reperfusion Injury by Attenuating Mitochondrial Apoptosis and Neuroinflammation via the TRAIL/DR4/DR5 Channel

Lihong Wen

892190815@qq.com

The Affiliated Hospital of Panzhihua University

Li He

The Affiliated Hospital of Panzhihua University

Yunyan Tao

The Affiliated Hospital of Panzhihua University

Li Su

The Affiliated Hospital of Panzhihua University

Xiaohui Zhan

The Affiliated Hospital of Panzhihua University

Chen Zhu

The Affiliated Hospital of Panzhihua University

Research Article

Keywords: Ischemic stroke, Electroacupuncture, TRAIL/DR4/DR5, Mitochondrial apoptosis, Neuroinflammation

Posted Date: November 23rd, 2026

DOI: https://doi.org/10.21203/rs.3.rs-11670764/v1

License: This work is licensed under a Creative Commons Attribution 4.0 International License.
Read Full License

Electroacupuncture Alleviates Cerebral Ischemia-Reperfusion Injury by Attenuating Mitochondrial Apoptosis and Neuroinflammation via the TRAIL/DR4/DR5 Channel

Lihong Wen[1], Li He[2], Yunyan Tao[1], Li Su[3], Xiaohui Zhan[1], Chen Zhu[1*]

[1]The Affiliated Hospital of Panzhihua University, Panzhihua, Sichuan, China

[2]The Affiliated Hospital of Panzhihua University, Panzhihua, Sichuan, China

[3]The Affiliated Hospital of Panzhihua University, Panzhihua, Sichuan, China

Lihong Wen,Department of Neurology, Ph.D., E-mail: 89219815@qq.com.

Li He,Medical Department, Master's, E-mail: lihe916@163.cn.

Yunyan Tao,Department of Neurology,Bachelor's, E-mail: 1692074838@qq.com.

Li Su, Department of critical care medicine, Master's, E-mail: 13982387080@163.com.

Xiaohui Zhan, Department of Neurology, Bachelor's,E-mail: 934241099@qq.com;.

Corresponding author: Chen Zhu,Department of Neurology, Master's, No. 27 Taoyuan Street, Dongqu District, Panzhihua City, Sichuan Province, 617000, China; E-mail: wenlihong@pzhxy.wecom.work; Tel: +86-13982349866.

Abstract

Objective: To integrate cross-species transcriptomic bioinformatics screening with in vivo animal experimental validation, systematically identify the core target genes regulated by electroacupuncture (EA) in ischemic stroke, and reveal the mechanism by which the TRAIL/DR4/DR5 signaling pathway mediates the protective effect of EA against cerebral ischemia-reperfusion injury.

Methods: Based on the human ischemic stroke dataset GSE16561 and the rat MCAO acupuncture intervention dataset GSE262257 from the GEO database, key candidate genes in stroke were screened through differential expression analysis and WGCNA. A cross-species three-way intersection was performed to identify acupuncture-reversed genes, which were then refined by three machine learning algorithms—LASSO, random forest, and SVM-RFE—to identify core hub genes and regulatory pathways. A 30-min transient middle cerebral artery occlusion (tMCAO) reperfusion model was established in rats in vivo, and the animals were randomly

divided into five groups. EA was applied at Shuigou (GV26) and bilateral Neiguan (PC6) with a 10/50 Hz dilatational wave for 3 consecutive days. Neurological injury was assessed, and the regulatory effects on the pathway were verified through behavioral tests, histological staining, and molecular biology experiments.

Results: A total of 17 acupuncture-reversed genes were identified, from which five core hub genes were screened. Among them, TNFSF10, which encodes the TRAIL protein, was a key regulatory node in the protein–protein interaction network. In vivo experiments confirmed that EA ameliorated neurological deficits, reduced cerebral infarct volume, and alleviated pathological damage in brain tissue; downregulated the expression of TRAIL, DR4, and DR5 in ischemic brain tissue; inhibited the activation of the mitochondrial apoptosis pathway; and decreased the levels of pro-inflammatory cytokines such as TNF-α, IL-1β, and IL-6. Sham EA exerted no significant protective effect, and exogenous supplementation with rhTRAIL reversed the anti-apoptotic and anti-inflammatory effects of EA.

Conclusion: EA alleviates cerebral ischemia-reperfusion injury by inhibiting the TRAIL/DR4/DR5 signaling pathway, thereby simultaneously blocking the mitochondrial apoptotic cascade and the amplification of neuroinflammation.

Keywords: Ischemic stroke; Electroacupuncture; TRAIL/DR4/DR5; Mitochondrial apoptosis; Neuroinflammation

Introduction

Stroke is one of the leading causes of death and disability worldwide. According to the World Stroke Organization, nearly 12 million new stroke cases occur globally each year [1, 2]. In China, ischemic stroke (IS) accounts for approximately 70%–80% of all stroke cases, and its pathological mechanisms are complex, involving energy metabolism failure, excitotoxicity, oxidative stress, neuroinflammation, and apoptosis [3, 4]. Currently, intravenous thrombolysis with recombinant tissue plasminogen activator (rt-PA) is a highly effective intervention for acute ischemic stroke [5]; however, its clinical benefit is limited to a small population due to the strict time window (within 4.5 hours of onset) and the risk of hemorrhagic transformation [6-8]. Therefore, identifying effective and safe adjuvant therapies to extend the thrombolytic time window and attenuate ischemia-reperfusion injury remains a research priority in the stroke field.

Acupuncture, an integral part of traditional Chinese medicine, is widely used in the clinical treatment and rehabilitation of stroke. The Xingnao Kaiqiao (regaining consciousness and opening the orifices) needling method, with Shuigou (GV26) and Neiguan (PC6) as the core acupoints, is a classic intervention for acute ischemic stroke [9, 10]. Multiple clinical and basic studies have confirmed that this needling method can improve microcirculation in the ischemic region, alleviate neurological injury, and potentially extend the time window for thrombolytic therapy [11]. Existing evidence suggests that the protective effect of EA on blood-brain barrier integrity and its regulation of the balance between autophagy and apoptosis are important mechanisms underlying its action against cerebral ischemia-reperfusion injury [12, 13]. However, the core regulatory networks and key target molecules of acupuncture in stroke have not yet been fully elucidated, which hinders the in-depth analysis of its mechanisms and the standardized clinical promotion of acupuncture [10, 13].

Tumor necrosis factor-related apoptosis-inducing ligand (TRAIL) and its death receptors DR4 and DR5 play a crucial role in mediating the extrinsic apoptotic signaling pathway [14, 15]. In acute myocardial infarction, aberrant activation of the TRAIL/DR4/DR5 pathway can induce neutrophil infiltration and the formation of

neutrophil extracellular traps, thereby aggravating cardiac ischemia-reperfusion injury [16]. In this study, based on the ischemic stroke dataset (GSE16561) and the rat MCAO model with acupuncture intervention dataset (GSE262257) from the NCBI GEO public database, we combined differential expression analysis, WGCNA, immune infiltration analysis, and machine learning to systematically screen for potential core reversal genes of EA [17]. At the animal experimental level, we established a rat MCAO model to evaluate the effects of acupuncture (or EA) intervention on neurological deficits, cerebral infarct volume, and pathological injury, and focused on investigating whether EA alleviates the neuroinflammatory response after cerebral ischemia-reperfusion injury by inhibiting TRAIL/DR4/DR5-mediated mitochondrial apoptosis, thereby providing a theoretical basis for the mechanistic interpretation and clinical promotion of acupuncture in the treatment of ischemic stroke.

Materials and Methods

Data acquisition and preprocessing

Gene expression profile datasets were downloaded from the Gene Expression Omnibus (GEO) database of the National Center for Biotechnology Information (NCBI). GSE16561 was converted to a gene-level expression matrix (17,494 genes) after Illumina probe annotation, and missing values were filled with row means. The RNA-seq count matrix of GSE262257 was normalized using DESeq2. All analyses were performed in R 4.5. For GSE16561, differential expression analysis between the Stroke group and the Control group was conducted using the limma package. Screening criteria were: adjusted P value (adj.P) < 0.05 and $|\log_2 FC| > 0.585$. The results for differentially expressed genes (DEGs) were visualized with a volcano plot and a hierarchical clustering heatmap.

Weighted gene co-expression network analysis (WGCNA)

A scale-free co-expression network was constructed for the top 5,000 most variable genes in the GSE16561 expression matrix using the WGCNA package. The correlations between module eigengenes (MEs) and seven functional trait scores (Stroke_status, Immune_activation, Neutrophil_activity, Inflammation, Apoptosis, Oxidative_stress, Microglia_activation) were assessed by Pearson correlation

coefficients, and significance was calculated using the corPvalueStudent function.

Candidate gene set construction and functional enrichment analysis

The 483 significant DEGs were intersected with genes in the stroke-positively correlated WGCNA modules (e.g., ME5, ME3). After probe-to-gene mapping, 93 candidate genes (96 probes corresponding to 93 unique gene symbols) were obtained as the core input set for subsequent analyses. Gene Ontology (GO) (BP/CC/MF) and Kyoto Encyclopedia of Genes and Genomes (KEGG) pathway enrichment analyses were performed on this gene set using the clusterProfiler package, with the pvalueCutoff set to 1.0 to retain the full results; the top 20 pathways are displayed in the figure. Immune infiltration of 12 immune cell types was assessed using the single-sample gene set enrichment analysis (ssGSEA) method (GSVA package), and intergroup differences were evaluated with the Wilcoxon rank-sum test.

Cross-species screening for acupuncture-reversed genes

Differential expression analysis using DESeq2 was performed for two comparisons in GSE262257 (Model vs. Sham, EA+rtPA vs. rtPA). Considering the wider dynamic range of RNA-seq compared to microarray, a more stringent threshold of $|\log_2 FC| > 1$ ($padj < 0.05$) was applied to the rat data. After gene names were unified to the human format using toupper(), a three-way Venn intersection was performed among the 93 human candidate genes, rat stroke model DEGs, and rat acupuncture intervention DEGs. The criterion for defining a reversed gene was: the gene met $|\log_2 FC| > 1$ and $padj < 0.05$ in both the stroke model group (Model vs. Sham) and the acupuncture intervention group (EA+rtPA vs. rtPA), and the $\log_2 FC$ signs in the two comparisons were opposite.

Machine learning screening for hub genes

Using the expression matrix of the 93 human stroke candidate genes as input features, three machine learning methods were introduced to further screen hub genes:(1) LASSO logistic regression, determining the optimal regularization parameter (λ.min) through 10-fold cross-validation to select genes with non-zero coefficients; (2) random forest (ntree = 1,000), ranking genes based on Mean Decrease Accuracy (MDA); (3) SVM-RFE, determining the optimal feature subset through recursive

feature elimination. The final hub gene set was determined based on the overlap across the three methods.

Animals

Specific pathogen-free (SPF) adult male Sprague-Dawley (SD) rats, weighing 220 ± 20 g, aged 6–8 weeks, were purchased from Beijing Vital River Laboratory Animal Technology Co., Ltd., with the animal production license number SCXK (Jing) 2021-0011. The rats were housed under SPF conditions in a controlled environment (22 ± 3 °C, 60% ± 5% humidity, 12-hour light/dark cycle) with ad libitum access to food and water. After an adaptive feeding period, the rats were randomly assigned to control and experimental groups for subsequent experiments. All animal experimental protocols were approved by the Animal Ethics Committee of The Affiliated Hospital of Panzhihua University (Approval No. PD2006006).

Rats were first anesthetized by isoflurane inhalation (5% for induction, 1.5–2% for maintenance). After fixation, a midline cervical incision was made to expose the right common carotid artery (CCA), external carotid artery (ECA), and internal carotid artery (ICA). The distal end of the ECA was ligated, and the CCA and ICA were temporarily clamped with micro-arterial clips to block blood flow. A small incision was made in the proximal wall of the ECA, and a standardized nylon filament was inserted through the incision and gently advanced along the ICA towards the cranium to a depth of approximately 18 mm until slight resistance was felt, indicating that the filament tip had reached the origin of the middle cerebral artery (MCA) and successfully blocked MCA blood flow. The filament was secured by ligating the ECA stump, and the muscle and skin were sutured layer by layer. The rats were placed on a heating pad until recovery [18]. After 30 minutes of ischemia, the rats were lightly anesthetized again, and the filament was gently withdrawn into the ECA stump to achieve MCA blood flow reperfusion; significant resistance upon withdrawal and the absence of abnormal convulsions were considered signs of successful reperfusion. The presence of right-sided Horner's syndrome, left forelimb flexion, and leftward circling during walking upon recovery were used as criteria for successful model establishment [19]. Using a random number table, the rats were divided into five groups

(n=6 per group): (1) Sham group: only carotid artery dissection and ligation were performed, without filament insertion or subsequent treatment. (2) MCAO group: subjected to the filament MCAO model without any EA or drug intervention. (3) EA group (MCAO+Acup): received EA treatment at specific time points after MCAO. (4) Sham EA group (MCAO+Sham-Acup): after MCAO, needling was performed at non-acupoint, non-meridian sites without connecting to the EA device, to exclude interference from mechanical stimulation and stress caused by the needling procedure itself. (5) EA + rhTRAIL group (MCAO+Acup+rhTRAIL): after MCAO, received EA treatment combined with rhTRAIL intervention. At the end of the experiments, all rats were euthanized by an intraperitoneal overdose of sodium pentobarbital (150 mg/kg) to collect brain tissues.

EA treatment

After modeling, rats were fixed in the prone position. According to the rat anatomical atlas and acupoint localization standards, Shuigou (GV26) and bilateral Neiguan (PC6) were selected: GV26 was located at the junction of the upper 1/3 and middle 1/3 of the rat's upper lip; bilateral PC6 were located 3 mm proximal to the wrist crease on the palmar side of the forelimbs, along the path of the median nerve. Acupuncture needles (specification: 0.25 mm × 13 mm, manufacturer: Beijing Zhongyan Taihe Medical Instrument Co., Ltd., China) were used. After needle insertion, the needles were connected to an EA device, and stimulation was delivered with a dilatational wave (10 Hz/50 Hz) for 30 minutes per session. The current intensity was adjusted to produce slight rhythmic local muscle twitching without obvious stress responses such as struggling or squealing, typically controlled between 0.5 and 1.0 mA. The first EA treatment was initiated after reperfusion on Day 0, followed by one fixed-time treatment daily for 3 consecutive days, ending one day before sample collection. Rats in the Sham, MCAO, and rt-PA alone groups were grasped and fixed for the same duration each day without EA stimulation to exclude operational stress interference.

Drug administration

rhTRAIL was administered by intracerebroventricular injection. After anesthesia, rats were fixed on a stereotaxic frame. Using bregma as the origin and referring to a rat

brain stereotaxic atlas, the coordinates for the right lateral ventricle were determined: 0.8 mm posterior to bregma, 1.5 mm lateral to the midline, and 3.8 mm ventral to the skull surface. After drilling a hole in the skull with a dental drill, rhTRAIL (dose: 5 μg per rat, dissolved in 5 μL of sterile saline) was slowly injected using a microsyringe at a rate of 1 μL/min. After injection, the needle was left in place for 5 minutes and then slowly withdrawn. The skull hole was sealed with bone wax, and the skin was sutured. Rats in the EA, MCAO, and Sham EA groups received an equal volume of sterile saline via the same intracerebroventricular injection method. All administrations were completed immediately after reperfusion.

Rotarod test

Rotarod adaptation training was conducted once daily for three days before modeling (-3 d to -1 d). Rats were placed on a rotarod fatigue apparatus, and the rotation speed was uniformly accelerated from 5 rpm to 40 rpm. The latency to fall off the rotating rod was recorded. Each rat was trained three times per session with a 30-minute interval between trials; rats that consistently failed to adapt were excluded. Formal tests were performed on Days 1, 2, and 3 post-modeling using the same method as in the training phase. Each rat was tested three times consecutively, and the average value was taken as the final result to assess motor coordination and neurological functional recovery.

Neurological deficit score

The neurological deficit score of the experimental animals was assessed using the classic Zea Longa grading method. Two "blinded" investigators independently scored appetite, activity, and neurological deficits. The order of testing the assigned tasks was random [20].

Measurement of cerebral infarct volume (TTC staining)

Three days after modeling, brains were extracted and rapidly frozen at -20 °C for 20 minutes. 2,3,5-triphenyltetrazolium chloride (TTC) staining was performed using 2% TTC solution (T8877, Sigma, USA) at 37 °C for 20 minutes. Brains were then fixed in 4% paraformaldehyde (PFA; C104188, China), and slice images were acquired using a macro-microscope (ZEISS Axio Zoom V16, Germany). Infarct area was

measured using ImageJ 1.52a software (National Institutes of Health, USA). Cerebral infarct volume was calculated as follows: percentage of edema-corrected hemispheric lesion volume = [total infarct volume − (ipsilateral hemisphere volume − contralateral hemisphere volume)] / contralateral hemisphere volume × 100%.

Hematoxylin and eosin (HE) staining

To histologically assess infarct volume, hematoxylin and eosin (HE) staining was performed. Brain tissues were cryosectioned into 15-μm-thick slices, with one slice taken every 500 μm. The staining procedure was performed using an HE staining kit (G1120, Solarbio, China). Brain sections were incubated in hematoxylin dye solution for 2–3 minutes, rinsed with distilled water, and washed to remove excess stain. Differentiation was performed using a differentiation solution for 10 seconds, followed by two washes in running tap water for 3 minutes each. Sections were then incubated in eosin dye solution for 10–15 seconds, followed by sequential dehydration in 75% ethanol, 85% ethanol, 95% ethanol, and 100% ethanol (I) for 3 seconds each, and then in 100% ethanol (II) for 1 minute. Sections were cleared in xylene solution twice for 1 minute each. Finally, slides were sealed with neutral mounting medium and observed under a stereomicroscope (ZEISS Axio Zoom V16, Germany).

Enzyme-linked immunosorbent assay (ELISA)

For in vivo experiments, cardiac blood was collected from rats 3 days after tMCAO and centrifuged at 3,000 × g for 15 minutes at room temperature to separate serum. After anesthesia, rats were perfused with normal saline via intracardiac injection to flush out the blood. Following perfusion, brain tissues were extracted for further analysis. For in vitro experiments, cell supernatants were collected after different experimental treatments. Cell supernatants, brain tissue samples, and serum samples were placed in buffer and homogenized on ice using an ultrasonic homogenizer (E0380, Shanghai Beyotime Biotechnology Co., Ltd., China) for 10 minutes. The homogenized samples were then centrifuged at 1,500 × g for 15 minutes to collect the supernatant. The expression levels of TNF-α (EH0302, FineTest, China), IL-6 (97068ES48, YEASEN, China), and IL-1β (E-EL-H0149, Elabscience, China) were

quantified using specific ELISA kits.

Reverse transcription-quantitative polymerase chain reaction (RT-qPCR)

Total RNA was extracted from cells and tissues using an RNA extraction kit (R0017M, Beyotime Biotech Inc., China) according to the manufacturer's protocol. RNA concentration and purity were assessed using a NanoDrop™ Eight spectrophotometer (912A1101, Thermo Fisher Scientific, China). Reverse transcription was performed using the SureScript™ First Strand cDNA Synthesis Kit (QP031, GeneCopoeia, China) with incubation at 42 °C for 30 minutes, followed by heating at 85 °C for 5 minutes to inactivate the reverse transcriptase and generate cDNA. Quantitative polymerase chain reaction (qPCR) was performed on a real-time PCR system (Agilent, Santa Clara, CA, USA). BlazeTaq™ SYBR Green qPCR Mix (QP056, GeneCopoeia, China) was used as the fluorescent dye, and the reaction program was set as follows: pre-denaturation at 95 °C for 30 seconds, followed by 40 cycles of denaturation at 95 °C for 10 seconds and annealing/extension at 60 °C for 30 seconds. The relative expression level of target genes was calculated using the $2^{(-\Delta\Delta Ct)}$ method, where ΔCt = Ct value of target gene − Ct value of reference gene, and $\Delta\Delta Ct$ = ΔCt of experimental group − ΔCt of control group. Primer sequences are detailed in Table S1.

Western blot

Protein was extracted from the ischemic ipsilateral cerebral hemisphere using radioimmunoprecipitation assay lysis buffer (R0020, Solarbio, China). Protein concentration in the supernatant was quantified using a bicinchoninic acid protein assay kit (23227, Thermo Scientific, China). Equal amounts of protein (25 μg) were separated by sodium dodecyl sulfate-polyacrylamide gel electrophoresis (SDS-PAGE) and transferred onto polyvinylidene difluoride membranes (03010040001, Millipore, MA, USA). Membranes were blocked with rapid protein-free blocking solution (AR0041, Wuhan Boster Biological Technology Co., Ltd., China) for 1 hour at room temperature and then incubated overnight at 4 °C with primary antibodies. After washing with Tris-buffered saline containing Tween-20, the membranes were incubated with goat anti-rabbit IgG (H+L) secondary antibody for 1 hour.

Chemiluminescent substrate solution (36224ES, Shanghai Yeasen Biotechnology Co., Ltd., China) was added and incubated for 10 seconds, and protein bands were detected using a chemiluminescence imaging system (LI-COR Biosciences, USA). Table S2 provides antibody details and dilution ratios.

Statistical analysis

Data were analyzed using GraphPad Prism 9.5.0 software. Measurement data are presented as mean ± standard deviation. For multiple group comparisons, one-way analysis of variance was performed, followed by Tukey's honestly significant difference test for post-hoc analysis. A P value < 0.05 was considered statistically significant.

Results

Transcriptomic molecular characteristics and key gene screening in ischemic stroke

Transcriptomic landscape analysis was performed based on the GSE16561 human ischemic stroke peripheral blood expression profile dataset (63 samples, including 39 stroke and 24 healthy controls). Principal component analysis showed a clear separation tendency between the stroke and control groups along the PC1 axis, suggesting systematic differences in transcriptomic characteristics between the two groups (Figure 1A). Using $|\log_2 FC| > 0.58$ and adjusted $P < 0.05$ as screening thresholds, a total of 483 DEGs were identified, comprising 362 upregulated and 121 downregulated genes. The volcano plot visually illustrates the overall distribution of up- and down-regulated genes (Figure 1B). A heatmap of the top 50 most significantly differentially expressed genes showed that samples from the two groups could be clearly clustered based on gene expression patterns, further validating the sample discrimination capacity of the DEGs (Figure 1C).

WGCNA was used to construct a gene co-expression network, and 10 gene co-expression modules were identified. The module-trait correlation analysis revealed that the ME5 module had the strongest positive correlation with stroke status ($r=0.74$, $P < 0.001$) and was also highly positively correlated with pathological traits such as inflammation, oxidative stress, and microglial activation, suggesting that genes in this

module are deeply involved in the pathological process of ischemic stroke (Figure 1D). By intersecting the DEGs with genes in the stroke-positively correlated modules, 93 key candidate genes for stroke were ultimately obtained. GO functional enrichment analysis showed that these genes were mainly enriched in biological processes such as the JNK cascade, reactive oxygen species metabolic process, and activation of innate immune response (Figure 1E).

The results of the ssGSEA immune infiltration analysis showed that, compared with the control group, the enrichment scores of immune cells including B cells, $CD4^+$ T cells, monocytes, macrophages, and neutrophils in the peripheral blood of the ischemic stroke group were significantly increased ($P < 0.01$ or $P < 0.001$), indicating that ischemic stroke is accompanied by systemic immune activation and remodeling of the inflammatory microenvironment (Figure 1F).

Cross-species identification and functional enrichment of acupuncture-reversed genes

To screen for ischemic stroke target genes that can be regulated by acupuncture intervention, the rat MCAO acupuncture intervention dataset GSE262257 was introduced for cross-species integrative analysis. Differential expression analysis showed that, compared with the sham group, 2,847 DEGs (1,244 upregulated and 1,603 downregulated) were identified in the MCAO model group (Figure 2A); compared with the rt-PA alone group, 2,167 DEGs were identified in the EA+rt-PA group (Figure 2B). A three-way intersection analysis of the 93 human stroke key genes, the rat MCAO model DEGs, and the rat acupuncture intervention DEGs yielded 17 intersecting genes (Figure 2C). Further verification of expression trends revealed that these 17 genes exhibited abnormal expression in the MCAO model, and their expression directions were completely reversed after acupuncture intervention, fitting the characteristic of a reversed gene as "dysregulated in disease and restored after intervention". Therefore, they were defined as acupuncture-reversed genes. A bidirectional bar chart visually displays the log_2FC changes of these 17 genes in the two comparisons; for example, CYP1B1 and PTGS2 were significantly upregulated in the model and downregulated after acupuncture, whereas TNFSF10 was

downregulated in the model and upregulated after acupuncture (Figure 2D).

KEGG pathway enrichment analysis of the 93 stroke key genes showed significant enrichment in pathways closely related to ischemic brain injury, such as apoptosis, NF-κB signaling pathway, and TNF signaling pathway, suggesting that acupuncture may exert neuroprotective effects by regulating the inflammation-apoptosis axis (Figure 2E).

Protein–protein interaction network analysis of acupuncture-reversed genes

To analyze the functional associations among the 17 acupuncture-reversed genes, a protein–protein interaction (PPI) network was constructed based on the STRING database. The adjacency matrix heatmap displays the interaction confidence scores between genes, with strong functional associations observed among multiple genes (Figure 3A). Connectivity analysis showed that PTGS2, TNFSF10, and ITGAM had high connectivity in the network and were core nodes of the interaction network (Figure 3B). Visualization of the PPI network revealed that the reversed genes formed functional interaction clusters centered on inflammatory regulation and apoptotic signaling, among which TNFSF10 (i.e., TRAIL), as a key ligand of the death receptor pathway, was located at a critical connection point in the network, suggesting that it may be an important target for the regulatory effects of acupuncture (Figure 3C).

Machine learning screening for core hub genes regulated by acupuncture

To further screen for core hub genes from the 17 acupuncture-reversed genes, three machine learning algorithms—LASSO logistic regression, random forest, and SVM-RFE—were employed for cross-screening. LASSO regression, through 10-fold cross-validation, selected 7 genes with non-zero coefficients at lambda.min, among which TNFSF10 and CYP1B1 had relatively high positive regression coefficients (Figure 4A, 4B). The random forest classifier had an out-of-bag error rate of 7.9%, and the importance ranking based on MDA showed that PLXDC2, BIRC2, and BAZ1A were the top three (Figure 4C). SVM-RFE analysis indicated that the model achieved optimal accuracy (approximately 95%) when the number of feature genes was 11 (Figure 4D).

The intersection of the results from the three methods yielded five commonly

identified core hub genes: BAZ1A, BIRC2, KPNB1, TNFSF10, and PLXDC2 (Figure 4E). The comprehensive hit score plot showed that these five genes were fully supported by all three methods, indicating high robustness of the screening results. Among them, TNFSF10, as the core gene of the TRAIL pathway, possesses both disease diagnostic value and acupuncture-response characteristics, making it a key candidate target for acupuncture regulation in ischemic stroke (Figure 4F).

Ameliorative effects of EA on neurological function and brain injury in MCAO rats

To verify the neuroprotective effect of EA and the mediating role of the TRAIL pathway, a 30-min tMCAO reperfusion model was established in rats, which were divided into sham, MCAO, EA, sham EA, and EA + rhTRAIL groups. The animal experimental design and intervention timeline are shown in Figure 5A. Behavioral test results showed that, compared with the sham group, the rotarod fall latency in the MCAO group was significantly shortened, and the neurological deficit score was significantly increased, indicating pronounced motor coordination deficits and neurological damage after modeling. Compared with the MCAO group, the EA group exhibited significantly prolonged rotarod latency and reduced neurological deficit scores, suggesting that EA effectively ameliorates neurological damage after cerebral ischemia-reperfusion. There was no significant difference between the sham EA group and the MCAO group, excluding interference from the mechanical stimulation of needling and handling stress. Compared with the EA group, the EA + rhTRAIL group showed a shortened rotarod latency and increased neurological deficit score, suggesting that exogenous rhTRAIL supplementation reversed the neuroprotective effects of EA (Figure 5B, 5C).

TTC staining results showed that the sham group had no obvious infarct lesions, whereas the MCAO group exhibited large pale infarct areas with a significantly increased percentage of infarct volume. Compared with the MCAO group, the cerebral infarct volume in the EA group was significantly reduced; the sham EA group showed no significant change in infarct volume; and the infarct volume in the EA + rhTRAIL group was significantly larger than that in the EA group, indicating that rhTRAIL counteracted the infarct-reducing effect of EA (Figure 6A).

Pathological observation with HE staining showed that neurons in the cortex of the sham group had regular morphology, orderly arrangement, and clear nucleoli. In the MCAO group, neurons were disorganized, with numerous cells exhibiting nuclear pyknosis, enhanced cytoplasmic eosinophilia, and accompanying inflammatory cell infiltration. In the EA group, the degree of neuronal damage was markedly alleviated, with relatively orderly cell arrangement and reduced necrotic cells and inflammatory infiltration. The sham EA group showed no significant difference in pathological injury compared to the MCAO group. In the EA + rhTRAIL group, neuronal damage was aggravated compared to the EA group, with an increase in necrotic cells (Figure 6B).

Regulation of the TRAIL/DR4/DR5-mediated mitochondrial apoptosis pathway by EA

Western blot analysis showed that, compared with the sham group, the protein expression levels of TRAIL and its receptors DR4 and DR5 in the brain tissue of the MCAO group were significantly increased. Compared with the MCAO group, the protein expression of TRAIL, DR4, and DR5 was significantly downregulated in the EA group ($P < 0.01$); there was no significant difference between the sham EA and MCAO groups. In contrast, the expression levels of TRAIL, DR4, and DR5 rebounded in the EA + rhTRAIL group compared to the EA group (Figure 7A). Detection of proteins related to the mitochondrial apoptosis pathway revealed that the expression of pro-apoptotic proteins Bax and Cleaved Caspase-3 was significantly increased, while the expression of the anti-apoptotic protein Bcl-2 was significantly decreased in the MCAO group. EA intervention reversed these changes by downregulating Bax and Cleaved Caspase-3 and upregulating Bcl-2. Sham EA did not exert a significant regulatory effect. After rhTRAIL supplementation, the regulatory effect of EA on apoptotic proteins was partially reversed, with Bax and Cleaved Caspase-3 expression rebounding and Bcl-2 expression decreasing (Figure 7B). These results suggest that EA exerts a neuroprotective effect by inhibiting the activation of the TRAIL/DR4/DR5 pathway, thereby suppressing the mitochondrial apoptotic

cascade.

Inhibitory effect of EA on neuroinflammation after cerebral ischemia-reperfusion

ELISA and qRT-PCR results showed that, compared with the sham group, the protein content and mRNA expression levels of pro-inflammatory cytokines TNF-α, IL-1β, and IL-6 in the brain tissue of the MCAO group were significantly increased, indicating that cerebral ischemia-reperfusion induced a robust neuroinflammatory response. Compared with the MCAO group, the protein and mRNA levels of these three inflammatory factors were significantly decreased in the EA group; no statistically significant difference was observed between the sham EA group and the MCAO group. Compared with the EA group, the expression levels of TNF-α, IL-1β, and IL-6 in the EA + rhTRAIL group rebounded significantly, indicating that rhTRAIL attenuates the anti-inflammatory effect of EA (Figure 8A-F). These results suggest that EA can mitigate the neuroinflammatory response induced by cerebral ischemia-reperfusion by inhibiting the TRAIL pathway.

Discussion

In this study, through cross-species transcriptomic integrative analysis and machine learning refinement, we identified for the first time 17 EA-specifically regulated reversal genes in ischemic stroke and pinpointed the TRAIL/DR4/DR5 signaling axis as a core candidate pathway. We further verified in vivo using a rat tMCAO model that EA alleviates cerebral ischemia-reperfusion injury by inhibiting the activation of the TRAIL/DR4/DR5 pathway, thereby simultaneously blocking the mitochondrial apoptotic cascade and the amplification of neuroinflammation.

The 17 reversal genes obtained in this study possess both disease relevance and acupuncture responsiveness, making them more valuable as intervention targets than simple disease-associated DEGs. Among them, PTGS2 (cyclooxygenase-2), a classic molecule mediating neuroinflammation, has been confirmed by multiple studies to be an important regulatory target of acupuncture against cerebral ischemic injury [21, 22]. Meanwhile, genes such as BAZ1A, KPNB1, and PLXDC2 have not been previously reported in acupuncture stroke research, which enriches the spectrum of molecular targets modulated by acupuncture and provides new directions for future studies.

The TRAIL-mediated death receptor pathway is one of the core pathways regulating apoptosis. Previous studies have shown that cerebral ischemia-reperfusion injury can induce the upregulation of TRAIL expression. Upon binding to its death receptors DR4 and DR5, TRAIL initiates extrinsic apoptosis by activating Caspase-8, and on the other hand, it triggers the cascade amplification of the mitochondrial apoptosis pathway by cleaving the Bid protein, ultimately leading to the massive death of neurons and cerebrovascular endothelial cells [23, 24]. Our results demonstrate that EA intervention significantly downregulates the protein expression of TRAIL, DR4, and DR5 in ischemic brain tissue, while inhibiting the activation of the key mitochondrial apoptosis molecule Bax, reducing the cleavage of Caspase-3, and upregulating the level of the anti-apoptotic protein Bcl-2, indicating that this may be an important mechanistic basis for its neuroprotective effects.

The biological functions of TRAIL are not limited to apoptosis induction. An increasing number of studies have shown that TRAIL can activate the NF-κB signaling pathway through the DR4 receptor, promoting the transcription and release of pro-inflammatory cytokines and participating in the occurrence and development of neuroinflammation [25, 26]. After cerebral ischemia-reperfusion, TRAIL-mediated apoptotic and inflammatory effects form a vicious cycle: TRAIL-induced cell death releases damage-associated molecular patterns (DAMPs), which further activate microglia to release inflammatory cytokines; the inflammatory microenvironment can in turn upregulate the expression of TRAIL and its receptors, exacerbating apoptosis, and collectively driving the progression of the ischemic penumbra towards the infarct core [27]. Our results show that EA intervention significantly reduces the protein and mRNA levels of pro-inflammatory cytokines such as TNF-α, IL-1β, and IL-6 in ischemic brain tissue, and that exogenous supplementation with rhTRAIL markedly attenuates the anti-inflammatory effect of EA. This finding suggests that the inhibitory effect of EA on neuroinflammation is also dependent on the regulation of the TRAIL/DR4/DR5 pathway.

This study has several limitations. First, pathway validation was only performed

through gain-of-function experiments with exogenous rhTRAIL, without further confirming the conclusions from a gene deficiency perspective using techniques such as gene knockout or RNA interference. Future studies could construct conditional DR4/DR5 knockout animal models to clarify the specific roles of the TRAIL pathway in different cell types. Second, this study only observed pathological changes in the acute phase 3 days after ischemia. The long-term regulatory effects of EA on the TRAIL pathway, as well as its impact on processes such as long-term neurological functional recovery and angiogenesis, remain to be further explored. Third, molecular detection in this study was performed at the whole brain tissue homogenate level, which could not delineate the expression differences and specific regulatory effects of the TRAIL/DR4/DR5 pathway in different cell types such as neurons, microglia, and cerebrovascular endothelial cells. Future studies could combine single-cell sequencing, immunofluorescence co-localization, and cell co-culture techniques to deeply analyze the intercellular signal interaction mechanisms. Fourth, this study only selected the two core acupoints Shuigou (GV26) and Neiguan (PC6). Whether other acupoints in the Xingnao Kaiqiao needling protocol exert synergistic effects through the same pathway still requires further comparative verification.

In conclusion, this study systematically screened and validated the TRAIL/DR4/DR5 pathway at the transcriptomic level as a key mediating target through which EA improves cerebral ischemia-reperfusion injury in vivo. EA can simultaneously block mitochondrial apoptosis and the neuroinflammatory cascade by inhibiting this pathway. These findings not only enrich the molecular mechanisms of acupuncture treatment for ischemic stroke but also provide experimental support and a new theoretical basis for the TRAIL pathway as a novel intervention target in stroke.

Acknowledgements

None.

Author contributions

Hongli Wen: Conceptualization, Methodology, Funding acquisition, Writing-original draft.

Li He: Data curation, Project administration.

Yunyan Tao: Investigation, Resources.

Li Su: Visualization,Project administration, Supervision.

Xiaohui Zhan: Data curation.

Chen Zhu: Supervision, Writing-review & editing.

Ethical Statement

This study was approved by the Animal Ethics Committee of Panzhihua University (Approval No. PD2006006).

Funding

This work was supported by the Science and Technology Project of Sichuan Provincial Administration of Traditional Chinese Medicine (Grant No. 26MSZX328) and the Project of China Panxi Health Industry Research Center (Grant No. 25PXKYCY0012).

Availability of data and materials

The data that support the findings of this study are available from the corresponding author upon reasonable request

Competing interests

The authors declare that they have no competing interests.

Clinical trial number: not applicable.

Supplementary Notes:

This manuscript has not been published elsewhere and is not under consideration by a nother journal.

This manuscript has not used artificial intelligence.

No reporting checklist was used.

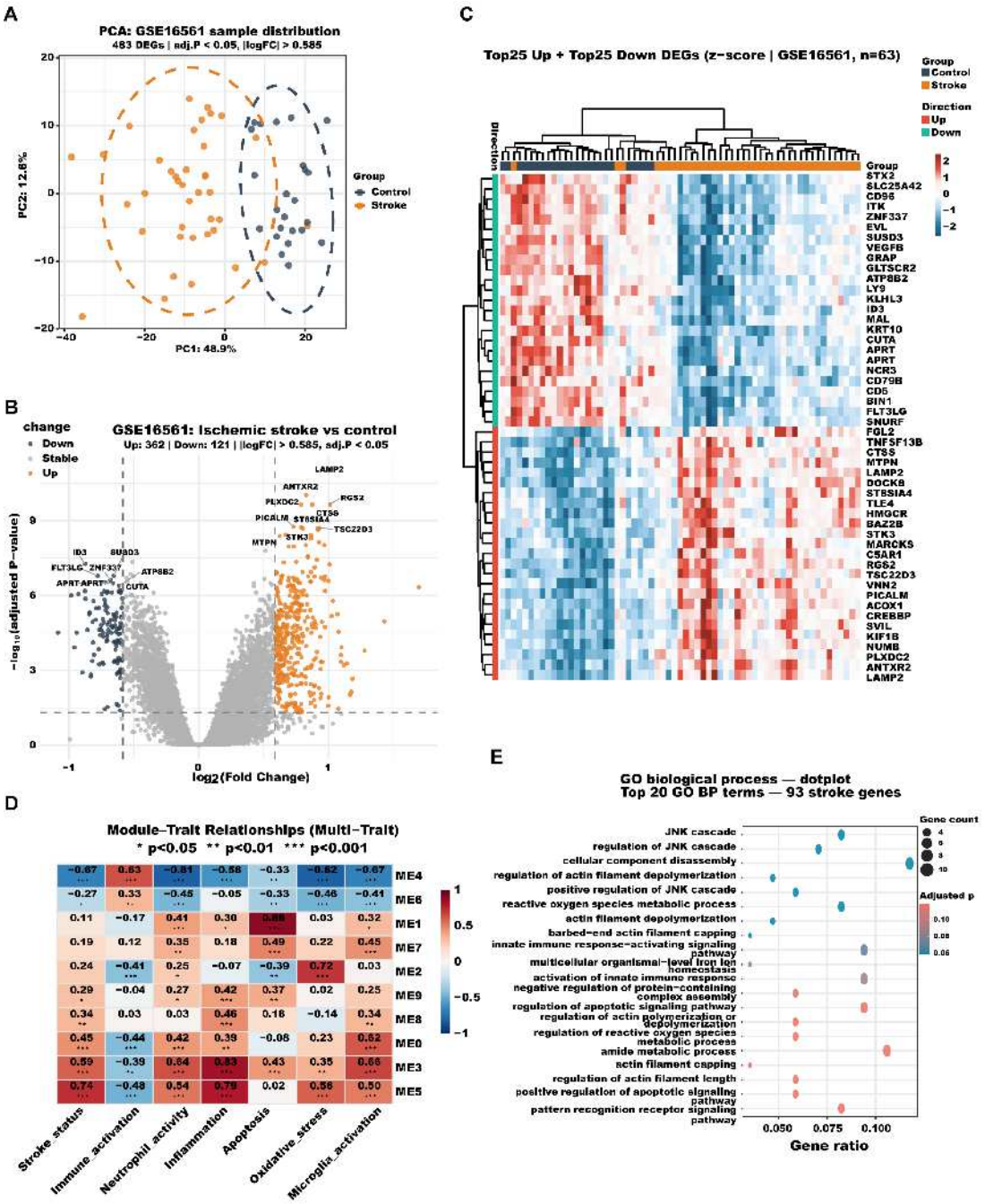

A
PCA: GSE16561 sample distribution
483 DEGs | adj.P < 0.05, |logFC| > 0.585
PC2: 12.6%
PC1: 48.9%
Group
Control
Stroke
B
change
Down
Stable
Up
GSE16561: Ischemic stroke vs control
Up: 362 | Down: 121 | |logFC| > 0.585, adj.P < 0.05
−log10(adjusted P−value)
log2(Fold Change)
C
Top25 Up + Top25 Down DEGs (z−score | GSE16561, n=63)
Group
Control
Stroke
Direction
Up
Down
D
Module−Trait Relationships (Multi−Trait)
* p<0.05 ** p<0.01 *** p<0.001
ME4
ME6
ME1
ME7
ME2
ME9
ME8
ME0
ME3
ME5
Stroke_status
Immune_activation
Neutrophil_activity
Inflammation
Apoptosis
Oxidative_stress
Microglia_activation
E
GO biological process — dotplot
Top 20 GO BP terms — 93 stroke genes
Gene count
Adjusted p
Gene ratio
F
Immune cell infiltration (ssGSEA)
GSE16561 | Stroke vs Control | 12 immune cell types
Group
Control
Stroke
ssGSEA enrichment score
B cells
CD4+ T cells
CD8+ T cells
NK cells
Monocytes
Macrophages
Dendritic cells
Neutrophils
Mast cells
Tregs
Plasma cells
Eosinophils

Figure 1. Differential expression analysis in the GSE16561 human stroke dataset

(A)PCA showing the overall distribution of samples from the control and stroke groups. (B) Volcano plot of DEGs, with upregulated genes shown in orange and downregulated genes in blue. (C) Heatmap of DEGs. (D) WGCNA module–trait relationship heatmap. (E) Bubble plot of GO BP enrichment for the 93 key stroke candidate genes. (F) Boxplots of ssGSEA infiltration scores for 12 immune cell subsets, comparing the immune microenvironment between the control and stroke groups.

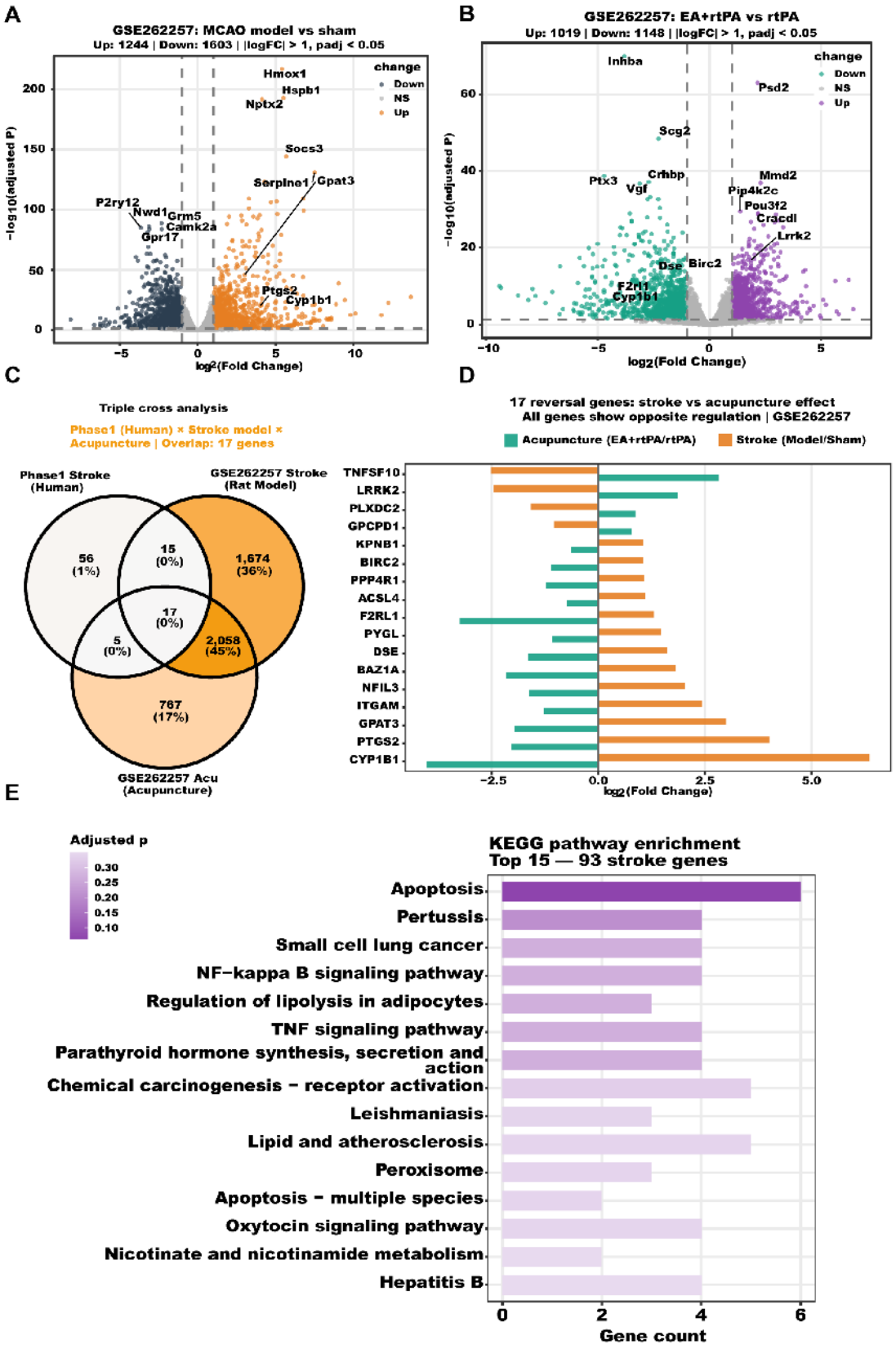


Figure 2. Cross-species identification and functional enrichment of acupuncture-reversed genes

(A) Volcano plot of DEGs for the MCAO model versus the sham group. (B) Volcano

plot of DEGs for the EA+rtPA versus the rtPA alone group. (C) Venn diagram of the three-way intersection analysis. (D) Log2 fold change (log2FC) of the 17 reversed genes in the two comparisons: “Model vs. Sham” (orange) and “EA+rtPA vs. rtPA” (teal). (E) Bar chart of KEGG pathway enrichment for the 93 key stroke candidate genes, displaying the top 15 most significant pathways.

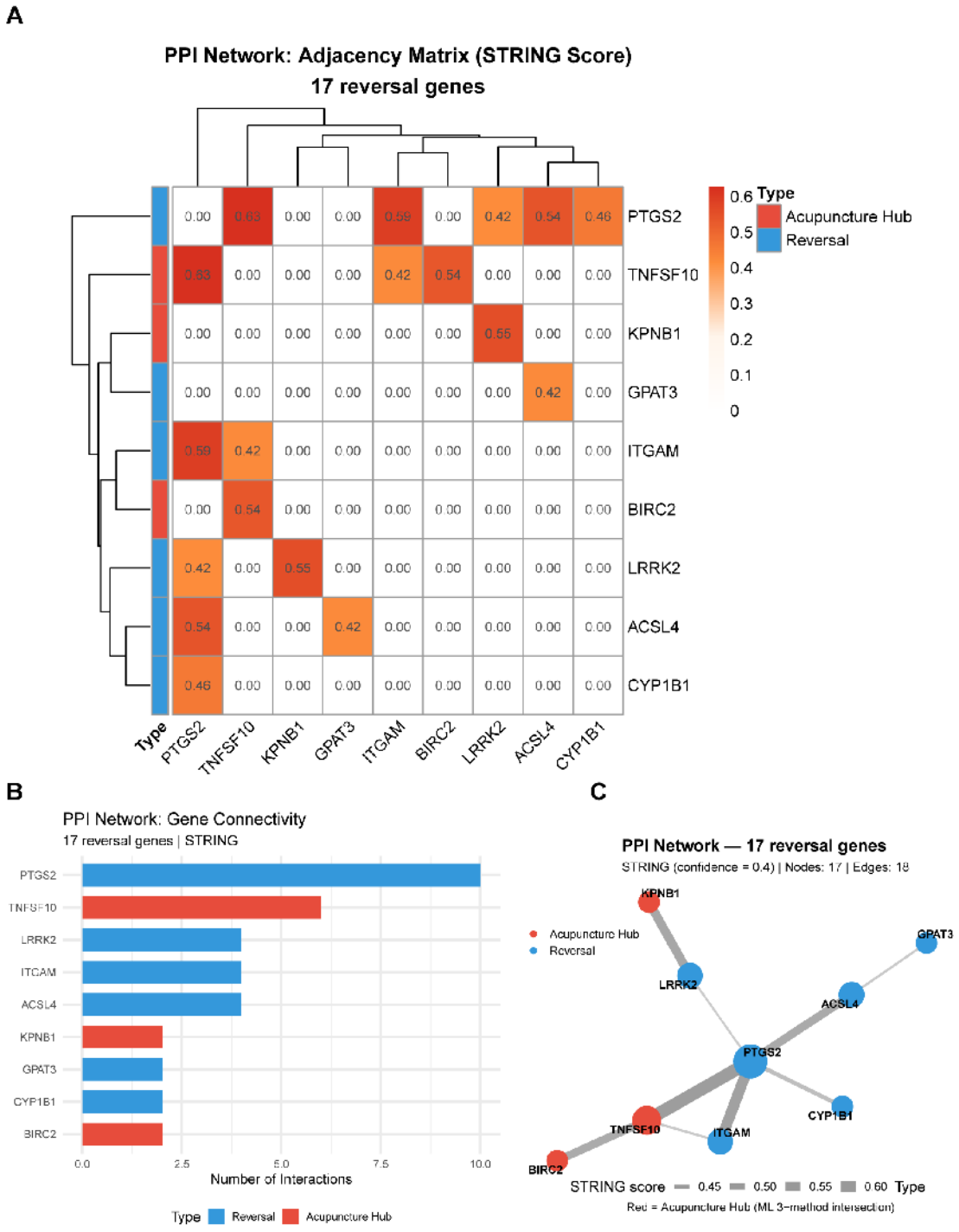


Figure 3. Protein–protein interaction (PPI) network analysis of

acupuncture-reversed genes

(A) Heatmap of the PPI adjacency matrix based on STRING scores. (B) Horizontal bar chart showing the connectivity levels of the 17 genes. (C) Visualization of the PPI network.

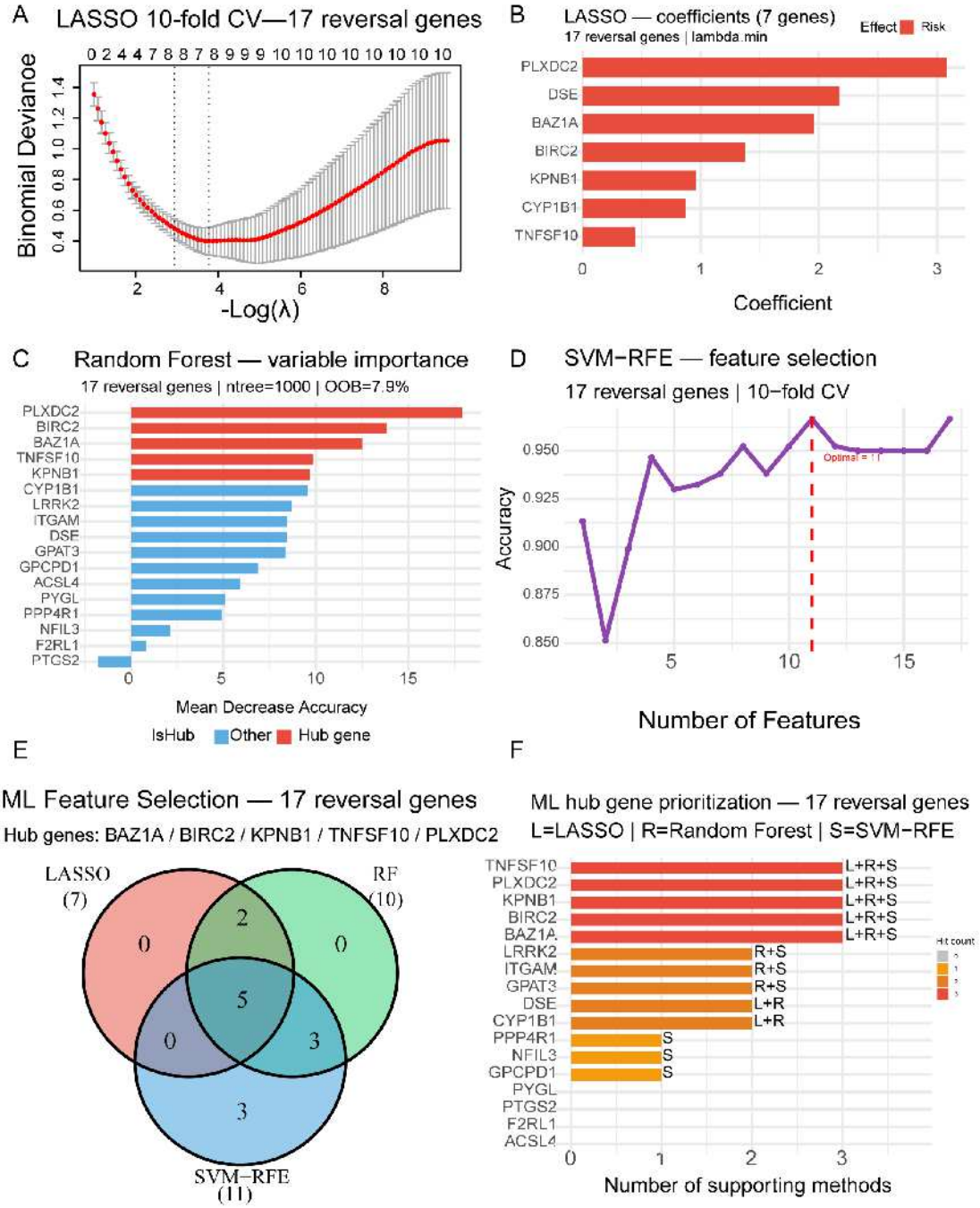


Figure 4. Machine learning-based refinement of hub genes from acupuncture-reversed genes

(A) LASSO 10-fold cross-validation curve. (B) Bar chart of genes with non-zero coefficients identified by LASSO. (C) Variable importance ranking from random

forest (RF). (D) SVM-RFE accuracy curve. (E) Venn diagram of the overlap among the three methods: LASSO, RF, and SVM-RFE. (F) Comprehensive hit score plot for the 17 reversed genes.

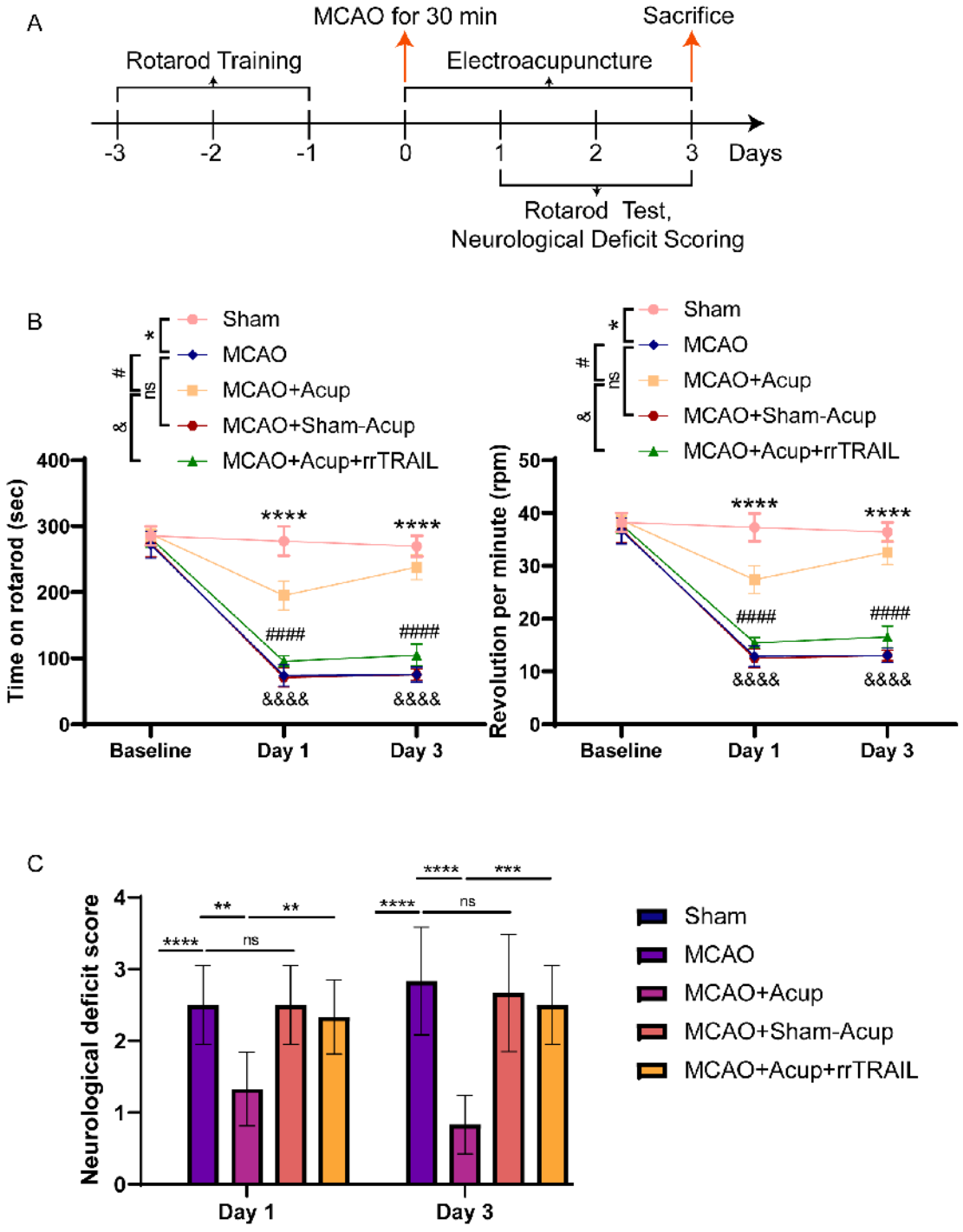


Figure 5. Ameliorative effect of electroacupuncture (EA) on neurological function in MCAO rats

(A) Schematic diagram of the experimental design and EA intervention timeline. (B)

Rotarod test results for rats in each group. (C) Neurological deficit scores for rats in each group on Day 1 and Day 3 post-modeling. (*p* < 0.05, **p* < 0.01, ***p* < 0.001)

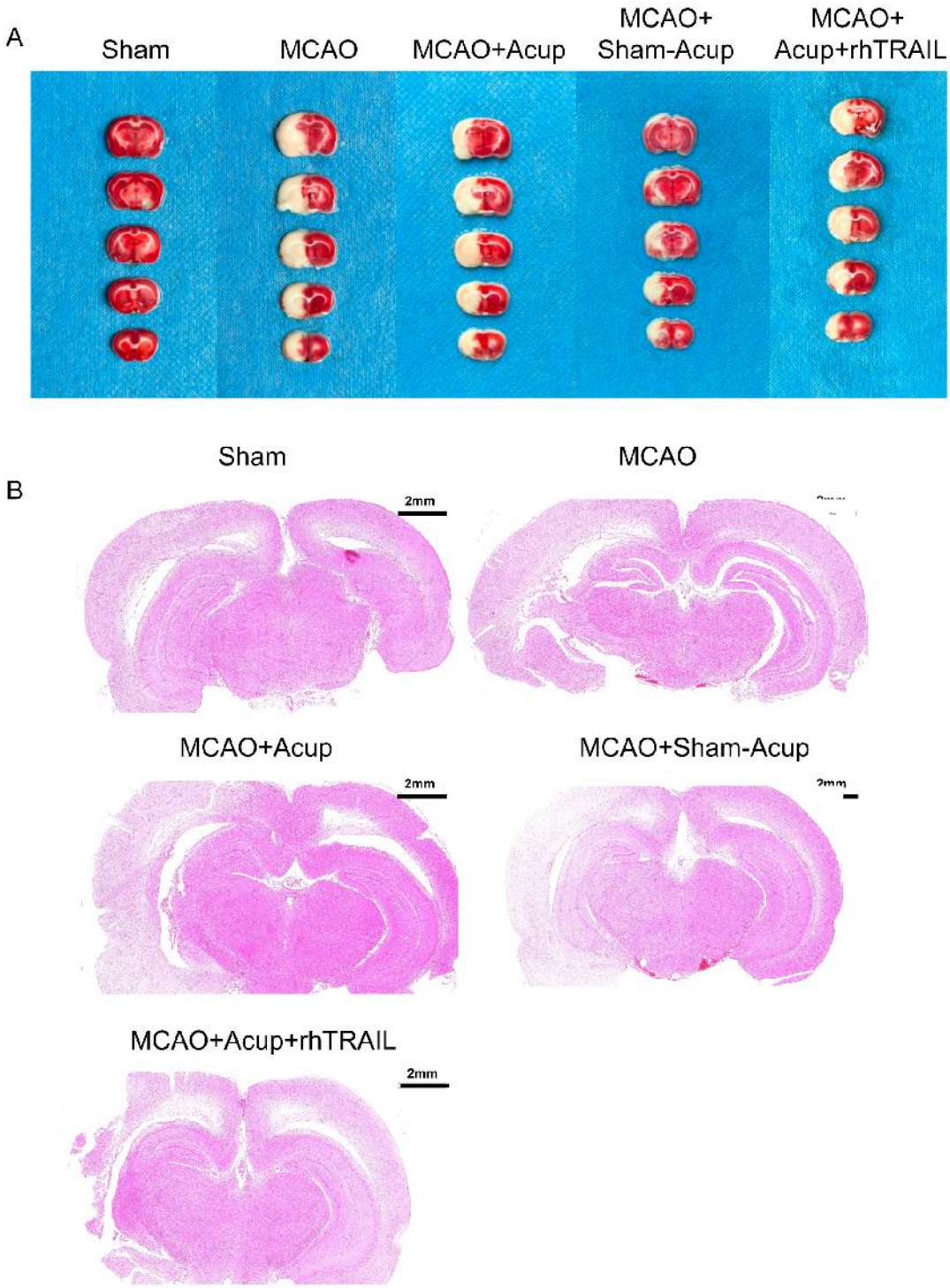


Figure 6. Ameliorative effect of EA on brain injury in MCAO rats

(A) Representative TTC-stained brain sections and quantitative analysis of the

percentage of cerebral infarct volume in each group (n=5). (B) Representative HE-stained brain sections from each group.

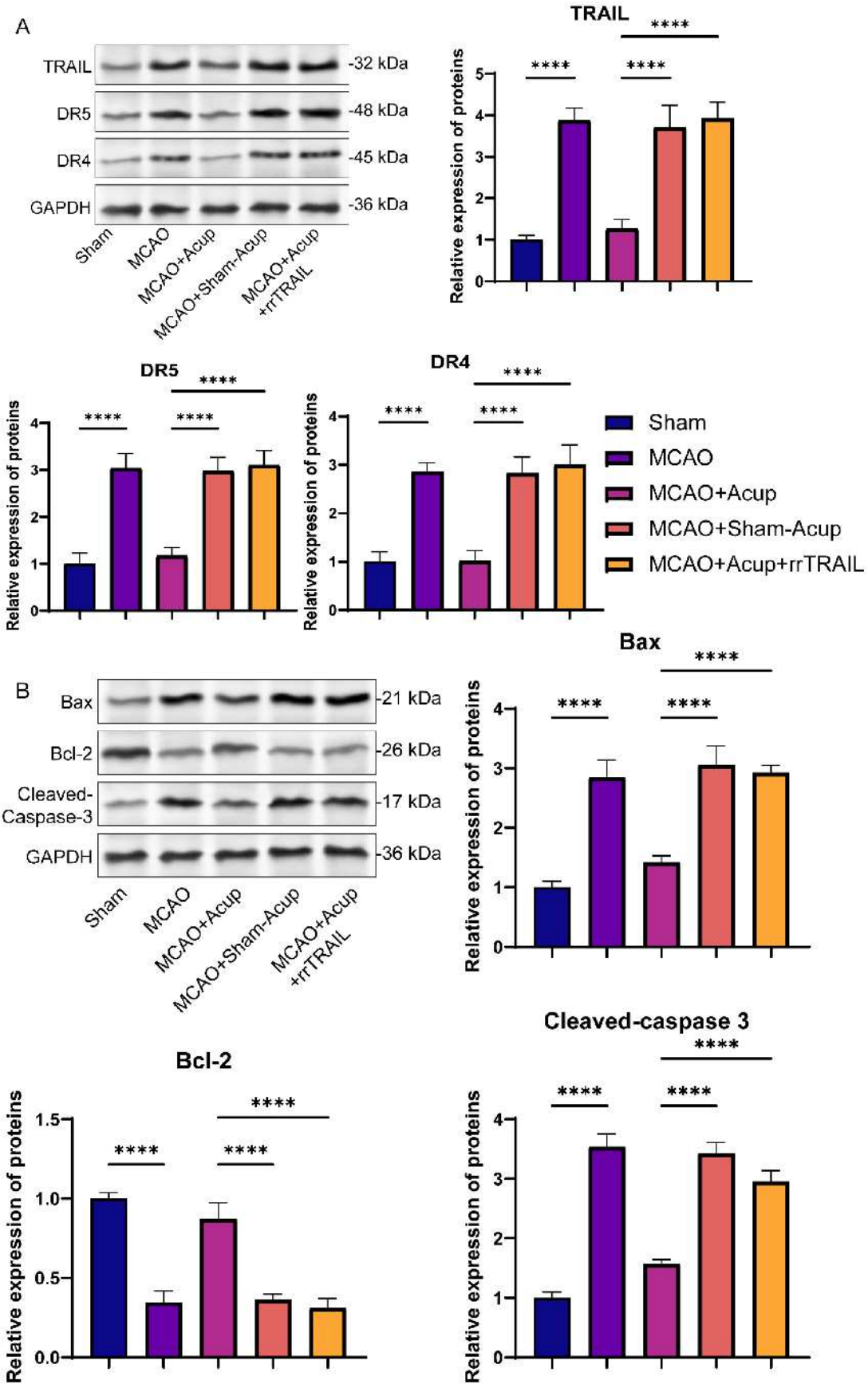


Figure 7. Regulation of the TRAIL/DR4/DR5-mediated mitochondrial apoptosis

pathway by EA

(A) Representative Western blot bands and relative densitometric quantification of TRAIL, DR4, and DR5 protein expression levels in brain tissue homogenates of rats in each group. (B) Representative Western blot bands and relative densitometric quantification of apoptosis-related proteins Bax, Bcl-2, and Cleaved Caspase-3 expression levels in brain tissue of rats in each group. (*p* < 0.05, **p* < 0.01, ***p* < 0.001)

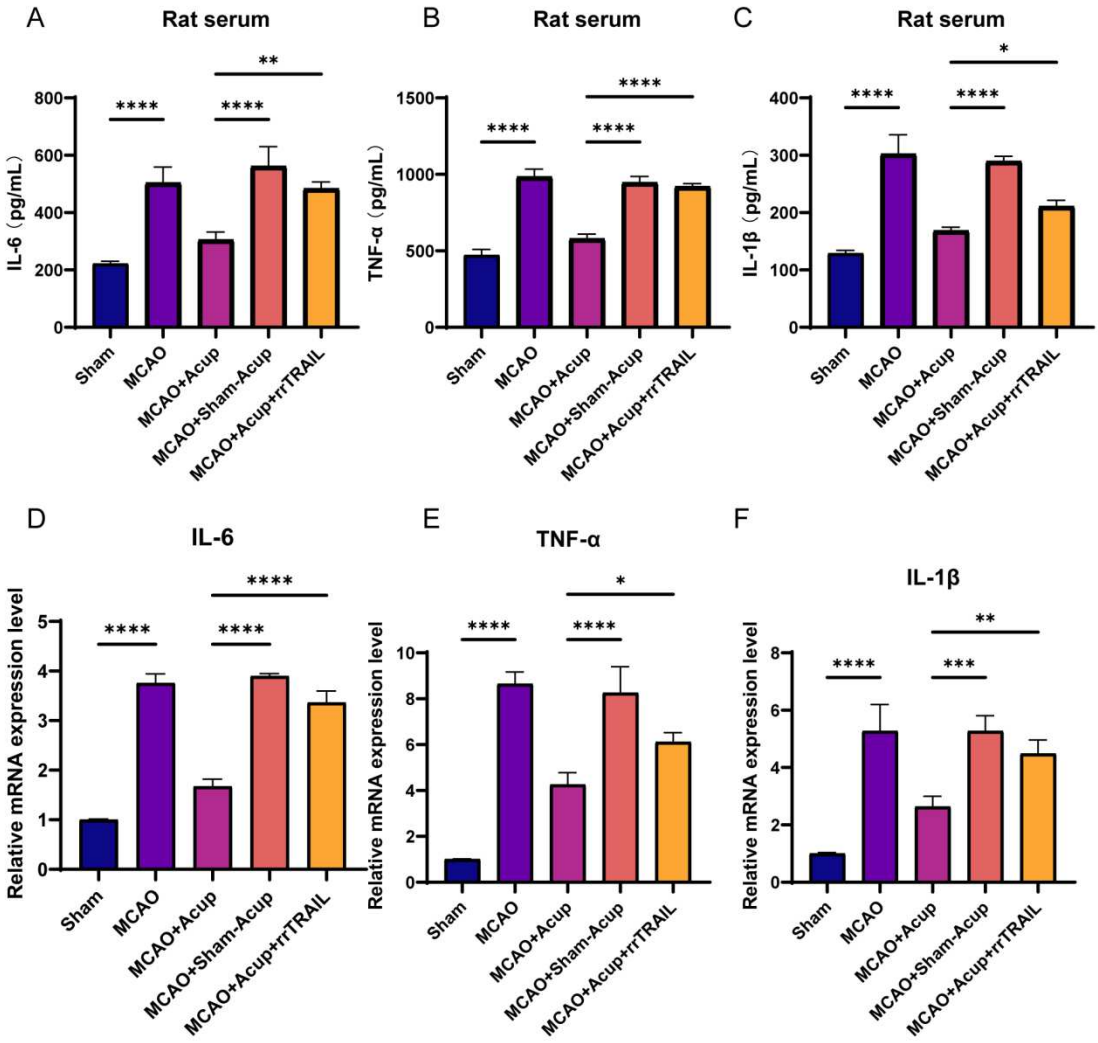


Figure 8. Inhibitory effect of EA on neuroinflammation after cerebral ischemia-reperfusion

(A-C) Quantitative bar charts of protein expression levels (determined by ELISA) of the pro-inflammatory cytokines IL-6, TNF-α and IL-1β in brain tissue homogenates

of rats in each group. (D-F) Quantitative bar charts of the relative mRNA expression levels (determined by qRT-PCR) of IL-6, TNF-α and IL-1β in brain tissue of rats in each group. (*p* < 0.05, **p* < 0.01, ***p* < 0.001)

References

1. Global, regional, and national burden of stroke and its risk factors, 1990-2021: a systematic analysis for the Global Burden of Disease Study 2021. *Lancet Neurol* 2024; 23: 973-1003. 2024/09/21. DOI: 10.1016/s1474-4422(24)00369-7.
2. Feigin VL, Brainin M, Norrving B, et al. World Stroke Organization: Global Stroke Fact Sheet 2025. *Int J Stroke* 2025; 20: 132-144. 2024/12/05. DOI: 10.1177/17474930241308142.
3. Wang W, Jiang B, Sun H, et al. Prevalence, Incidence, and Mortality of Stroke in China. *Circulation* 2017; 135: 759-771. DOI: doi:10.1161/CIRCULATIONAHA.116.025250.
4. Yenari MA, Kauppinen TM, Swanson RA. Microglial activation in stroke: therapeutic targets. Neurotherapeutics 2010;7:378-391. doi:10.1016/j.nurt.2010.07.005.
5. Emberson J, Lees KR, Lyden P, et al. Effect of treatment delay, age, and stroke severity on the effects of intravenous thrombolysis with alteplase for acute ischaemic stroke: a meta-analysis of individual patient data from randomised trials. *Lancet* 2014; 384: 1929-1935. 2014/08/12. DOI: 10.1016/s0140-6736(14)60584-5.
6. Lo EH, Dalkara T and Moskowitz MA. Mechanisms, challenges and opportunities in stroke. *Nat Rev Neurosci* 2003; 4: 399-415. 2003/05/03. DOI: 10.1038/nrn1106.
7. Ren X, Gao X, Li Z, et al. Electroacupuncture ameliorates neuroinflammation by inhibiting TRPV4 channel in ischemic stroke. *CNS Neurosci Ther* 2024; 30: e14618. 2024/02/09. DOI: 10.1111/cns.14618.
8. Sacks D, Baxter B, Campbell BCV, et al. Multisociety Consensus Quality Improvement Revised Consensus Statement for Endovascular Therapy of Acute Ischemic Stroke. *Int J Stroke* 2018; 13: 612-632. 2018/05/23. DOI: 10.1177/1747493018778713.
9. Yang X-Y, Zhu L-L, Zhong H, et al. Effect of xingnao kaiqiao acupuncture therapy for patient with acute ischemic stroke and the establishment of prediction model for prognosis. *World Journal of Acupuncture - Moxibustion* 2023; 33: 102-110. DOI: https://doi.org/10.1016/j.wjam.2023.02.004.
10. Yang ZX, Xie JH, Liu YP, et al. Systematic review of long-term Xingnao Kaiqiao needling effcacy in ischemic stroke treatment. *Neural Regen Res* 2015; 10: 583-588. 2015/07/15. DOI: 10.4103/1673-5374.155431.
11. Zhang ZH, Zhang XC and Ni GX. [Thrombolysis combined with acupuncture therapy for acute cerebral infarction: a Meta-analysis of randomized controlled trials]. *Zhen Ci Yan Jiu* 2021; 46: 431-438. 2021/06/05. DOI: 10.13702/j.1000-0607.200559.
12. Zhang Z, Lu T, Li S, et al. Acupuncture Extended the Thrombolysis Window by Suppressing Blood-Brain Barrier Disruption and Regulating Autophagy-Apoptosis Balance after Ischemic Stroke. *Brain Sci* 2024; 14 2024/04/27. DOI: 10.3390/brainsci14040399.

13. Li G, Li X, Dong J, et al. Electroacupuncture Ameliorates Cerebral Ischemic Injury by Inhibiting Ferroptosis. *Front Neurol* 2021; 12: 619043. 2021/03/26. DOI: 10.3389/fneur.2021.619043.
14. Ashkenazi A and Dixit VM. Apoptosis control by death and decoy receptors. *Curr Opin Cell Biol* 1999; 11: 255-260. 1999/04/21. DOI: 10.1016/s0955-0674(99)80034-9.
15. Montinaro A and Walczak H. Harnessing TRAIL-induced cell death for cancer therapy: a long walk with thrilling discoveries. *Cell Death Differ* 2023; 30: 237-249. 2022/10/05. DOI: 10.1038/s41418-022-01059-z.
16. Wang X, Xie R, Zhao D, et al. Blocking the TRAIL-DR5 Pathway Reduces Cardiac Ischemia-Reperfusion Injury by Decreasing Neutrophil Infiltration and Neutrophil Extracellular Traps Formation. *Cardiovasc Drugs Ther* 2025; 39: 983-999. 2024/06/20. DOI: 10.1007/s10557-024-07591-z.
17. Carmona-Mora P, Knepp B, Jickling GC, et al. Monocyte, neutrophil, and whole blood transcriptome dynamics following ischemic stroke. *BMC Med* 2023; 21: 65. 2023/02/22. DOI: 10.1186/s12916-023-02766-1.
18. Feng C, Wan H, Zhang Y, et al. Neuroprotective Effect of Danhong Injection on Cerebral Ischemia-Reperfusion Injury in Rats by Activation of the PI3K-Akt Pathway. *Front Pharmacol* 2020; 11: 298. 2020/03/29. DOI: 10.3389/fphar.2020.00298.
19. Longa EZ, Weinstein PR, Carlson S, et al. Reversible middle cerebral artery occlusion without craniectomy in rats. *Stroke* 1989; 20: 84-91. 1989/01/01. DOI: 10.1161/01.str.20.1.84.
20. Ifergane G, Boyko M, Frank D, et al. Biological and Behavioral Patterns of Post-Stroke Depression in Rats. *Can J Neurol Sci* 2018; 45: 451-461. 2018/06/09. DOI: 10.1017/cjn.2017.302.
21. Cheng N, Cheng X, Tan F, et al. Electroacupuncture attenuates cerebral ischemia/reperfusion injury by regulating oxidative stress, neuronal death and neuroinflammation via stimulation of PPAR-γ. *Acupunct Med* 2024; 42: 133-145. 2024/02/14. DOI: 10.1177/09645284231211600.
22. Zhao L, Liu L, Xu X, et al. Electroacupuncture Inhibits Hyperalgesia by Alleviating Inflammatory Factors in a Rat Model of Migraine. *J Pain Res* 2020; 13: 75-86. 2020/02/06. DOI: 10.2147/jpr.S225431.
23. Wang C and Youle RJ. The role of mitochondria in apoptosis*. *Annu Rev Genet* 2009; 43: 95-118. 2009/08/08. DOI: 10.1146/annurev-genet-102108-134850.
24. Li H, Zhu H, Xu CJ, et al. Cleavage of BID by caspase 8 mediates the mitochondrial damage in the Fas pathway of apoptosis. *Cell* 1998; 94: 491-501. 1998/09/04. DOI: 10.1016/s0092-8674(00)81590-1.
25. Chyuan IT and Hsu PN. TRAIL regulates T cell activation and suppresses inflammation in autoimmune diseases. *Cell Mol Immunol* 2020; 17: 1281-1283. 2020/03/27. DOI: 10.1038/s41423-020-0410-2.
26. Zhang J, Zheng Y, Luo Y, et al. Curcumin inhibits LPS-induced neuroinflammation by promoting microglial M2 polarization via TREM2/ TLR4/ NF-κB pathways in BV2 cells. *Mol Immunol* 2019; 116: 29-37. 2019/10/08. DOI: 10.1016/j.molimm.2019.09.020.

27. Jayaraj RL, Azimullah S, Beiram R, et al. Neuroinflammation: friend and foe for ischemic stroke. *J Neuroinflammation* 2019; 16: 142. 2019/07/12. DOI: 10.1186/s12974-019-1516-2.